Electronic Supplementary Material (ESI) for Physical Chemistry Chemical Physics.

Supporting Information

Melting of nucleobases. Getting the cutting edge of "Walden's Rule"

Amir Abdelaziz, Dzmitry H. Zaitsau, Natalia V. Kuratieva, Sergey P. Verevkin, and Christoph Schick*

Table of Contents

SI1 Specific heat capacity determination of nucleobases in the solid state

Fig. S1 shows the plot of specific heat capacity versus temperature obtained for the five nucleobases (uracil, thymine, cytosine, adenine and guanine) together with existing data published in the literature.[1-4]

The temperature ranges where comparison is possible between all the nucleobases heat capacities is narrow (230 K - 300 K). We can observe a quit good agreement between our experimental data and the literature ones in this temperature range, **Fig. S1**. Specific heat capacities measured for uracil, cytosine and guanine are in very good agreement with the literature data.[1-3] However, for adenine [1,2,4] the agreement was at the level of 3%. Heat capacity temperature dependence for thymine was measured for the first time.

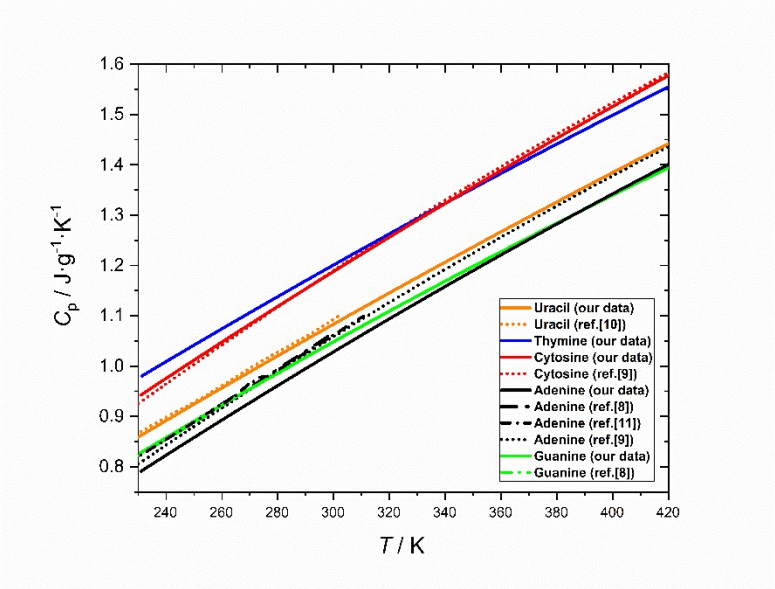

Fig. S1 Specific heat capacity vs temperature for the five nucleobases between 230 K and 420 K measured by DSC compared with the existing literature data.

Table S1 Experimental specific heat capacities c_p of nucleobases measured in this work.

T / K	c_p / J·K^{-1}·g^{-1} [a]				
	uracil	thymine	cytosine	adenine	guanine
230	0.976	0.859	0.939	0.825	0.788
240	1.009	0.892	0.976	0.858	0.823
250	1.042	0.924	1.012	0.891	0.858
260	1.074	0.957	1.048	0.923	0.893
270	1.106	0.989	1.084	0.955	0.927
280	1.138	1.021	1.119	0.986	0.962
290	1.170	1.052	1.154	1.018	0.995
300	1.201	1.084	1.188	1.049	1.029

310	1.232	1.115	1.223	1.079	1.062
320	1.263	1.146	1.256	1.109	1.094
330	1.293	1.176	1.290	1.139	1.127
340	1.324	1.207	1.323	1.169	1.158
350	1.354	1.237	1.356	1.198	1.190
360	1.383	1.267	1.389	1.227	1.221
370	1.413	1.297	1.421	1.256	1.252
380	1.442	1.326	1.453	1.284	1.283
390	1.470	1.356	1.485	1.312	1.313
400	1.499	1.385	1.516	1.340	1.343
410	1.527	1.414	1.547	1.367	1.372
420	1.555	1.442	1.578	1.394	1.401

[a] Expanded uncertainty (0.95 confidence level, k=2) of the heat capacity is $U(c_p) = 0.03\ c_p$.

SI2 Fusion enthalpy determination

The resulting fusion enthalpy $\Delta_{fus}H^0(T_{fus})$ corresponding to their respective sample mass m_s, the set of data (summarized in **Table S2**) was linearly fitted and the resulting slope correspond to the specific fusion enthalpy (in $J \cdot g^{-1}$). The complete description of the mass evaluation procedure can be found in previous publications.[5,6]

Table S2 Summarized values of the fusion enthalpy $\Delta_{fus}H^0(T_{fus})$ with the corresponding sample mass for uracil, thymine, adenine and guanine. Experimental data for cytosine are published elsewhere.[5]

uracil		thymine		adenine		guanine	
m_s / ng	$\Delta_{fus}H^0(T_{fus})$ /μJ	m_s / ng	$\Delta_{fus}H^0(T_{fus})$ /μJ	m_s / ng	$\Delta_{fus}H^0(T_{fu}$ /μJ	m_s / ng	$\Delta_{fus}H^0(T_{fus}$ /μJ
13.7 ± 0.2	4.4 ± 0.5	6.8 ±0.2	1.9 ± 0.2	6.7 ± 0.2	1.6 ± 0.3	5.9 ± 1.0	2.3 ± 0.2
17.9 ± 0.4	6.1 ± 0.5	6.1 ± 0.2	1.4 ± 0.2	7.2 ± 0.1	1.7 ± 0.3	1.5 ± 0.3	0.6 ± 0.2
13.0 ± 0.4	3.8 ± 0.5	8.9 ± 0.2	2.5 ± 0.2	9.0 ± 0.2	2.1 ± 0.3	1.0 ± 0.4	0.4 ± 0.2
9.4 ± 0.3	3.1 ± 0.5	5.7 ± 0.2	1.6 ± 0.2	15.4 ± 0.2	3.9 ± 0.3	1.8 ± 0.3	0.8 ± 0.2
21.3 ± 0.4	7.7 ± 0.5	6.4 ± 0.3	1.6 ± 0.2	7.6 ± 0.2	1.8 ± 0.3	1.4 ± 0.5	0.4 ± 0.2
13.8 ± 0.4	4.3 ± 0.5	6.4 ± 0.2	1.6 ± 0.2	8.2 ± 0.2	1.9 ± 0.3	3.4 ± 0.5	1.3 ± 0.2
10.9 ± 0.5	3.2 ± 0.5	10.1 ± 0.2	2.7 ± 0.2	7.9 ± 0.1	2.2 ± 0.3	2.5 ± 0.4	0.9 ± 0.2
12.5 ± 0.3	4.1 ± 0.5	6.0 ± 0.2	1.8 ± 0.2	10.0 ± 0.2	2.8 ± 0.3	1.4 ± 0.3	0.5 ± 0.2
12.5 ± 0.4	4.0 ± 0.5	7.3 ± 0.2	1.9 ± 0.2	10.7 ± 0.2	3.0 ± 0.3	2.8 ± 0.4	1.2 ± 0.2
11.7 ± 0.4	4.3 ± 0.5	6.4 ± 0.2	1.8 ± 0.2	6.4 ± 0.2	1.5 ± 0.3	2.9 ± 0.4	1.1 ± 0.2
10.3 ± 0.4	3.3 ± 0.5	11.2 ± 0.3	3.1 ± 0.2	11.5 ± 0.2	3.1 ± 0.3	2.6 ± 0.4	0.8 ± 0.2

11.6 ± 0.4	3.5 ± 0.5	8.7 ±0.2	2.5 ± 0.2	5.2 ± 0.2	1.2 ± 0.3	1.4 ± 0.4	0.4 ± 0.2
12.7 ± 0.4	4.1 ± 0.5	9.1 ± 0.1	2.3 ± 0.2				
6.6 ± 0.3	2.1 ± 0.5	5.4 ± 0.2	1.3 ± 0.2				
9.8 ± 0.3	3.0 ± 0.5	15.0 ± 0.3	3.8 ± 0.2				
14.3 ± 0.4	4.8 ± 0.5	11.0 ±0.3	2.8 ± 0.2				
8.6 ± 0.3	2.8 ± 0.5						

SI3 Interplay between melting and thermal decomposition

Synthetic chemists regard the capillary method as the standard technique for melting point determination. In this method, a thin glass capillary tube is filled with the sample and it is introduced into a heated block with accurately measured temperature. The temperature in the heating block is ramped at a fixed rate until the sample melt. The detection of the melting begin is performed visually or recorded with optical methods. More informative, precise and commonly used method is differential scanning calorimetry (DSC). In this method, a sample is encapsulated in a metal pan and heated/cooled with a certain scanning rate. The extrapolated peak onset temperature of the DSC-peak corresponds to the melting point and the area of the melting peak is referenced to the fusion enthalpy (the word fusion means the same thing as "melting").[7] Heating and cooling rates in DSC are commonly limited to about 10 $K \cdot s^{-1}$. At such rates decomposition of organic samples is often observed below or during melting.[8]

The FSC melting at much higher heating rates indicate that the samples were chemically stable during the study. Nevertheless, to assure the pure melting nature of the observed transition we studied the decomposition kinetics of the compounds under investigation. We applied low heating rate TGA scans to evaluate the decomposition kinetic parameters (E_α, A_α, $g(\alpha)$) by using isoconversional kinetic analysis.[9]

Typical TGA curves were measured for the thermal decomposition of nucleobases under non-isothermal conditions (heating rates of 2, 10 and 25 $K \cdot min^{-1}$ were applied). The use of such slow heating rates results in TGA data corresponding to the thermal decomposition occurring in the solid-state (see **Fig. S2**).

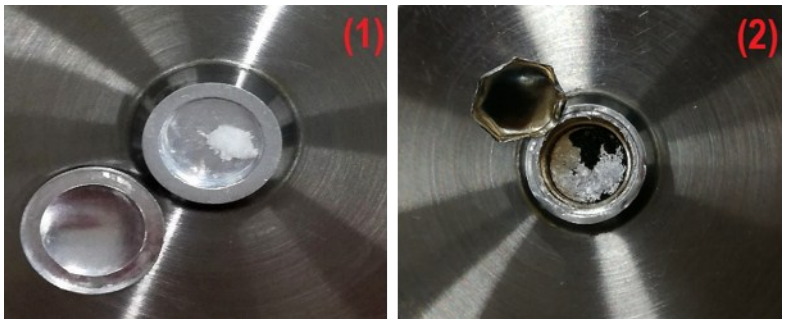

Fig. S2 Photography of TGA aluminum pan before (1) and after (2) thermal decomposition of guanine (change from white to black color).

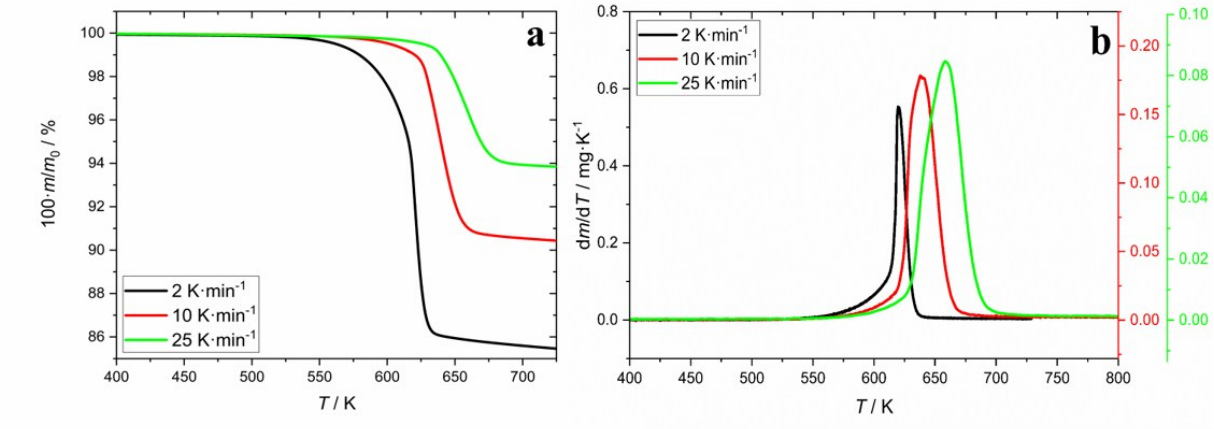

Fig. S3 TGA and corresponding DTG curves for the thermal decomposition of uracil under linear non-isothermal conditions and under N_2 flow (200 ml·min^{-1}).

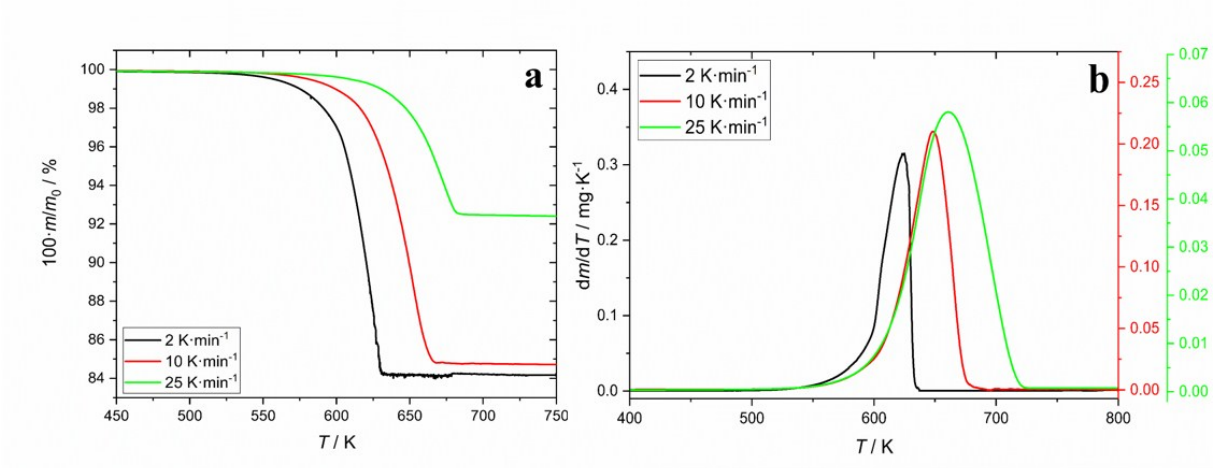

Fig. S4 TGA and corresponding DTG curves for the thermal decomposition of thymine under linear non-isothermal conditions and under N_2 flow (200 ml·min^{-1}).

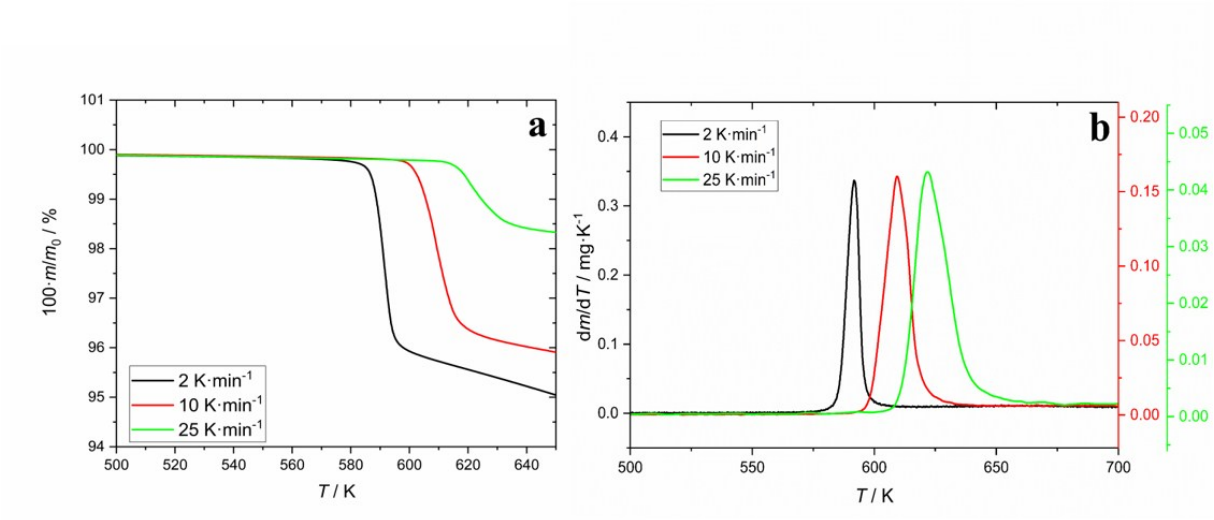

Fig. S5 TGA and corresponding DTG curves for the thermal decomposition of cytosine under linear non-isothermal conditions and under N_2 flow (200 ml·min^{-1}).

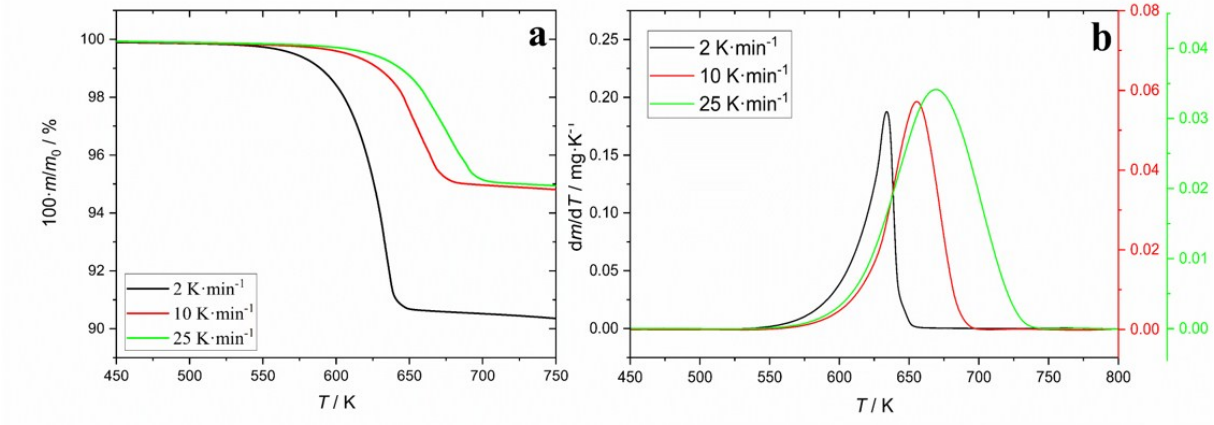

Fig. S6 TGA and corresponding DTG curves for the thermal decomposition of adenine under linear non-isothermal conditions and under N_2 flow (200 ml·min^{-1}).

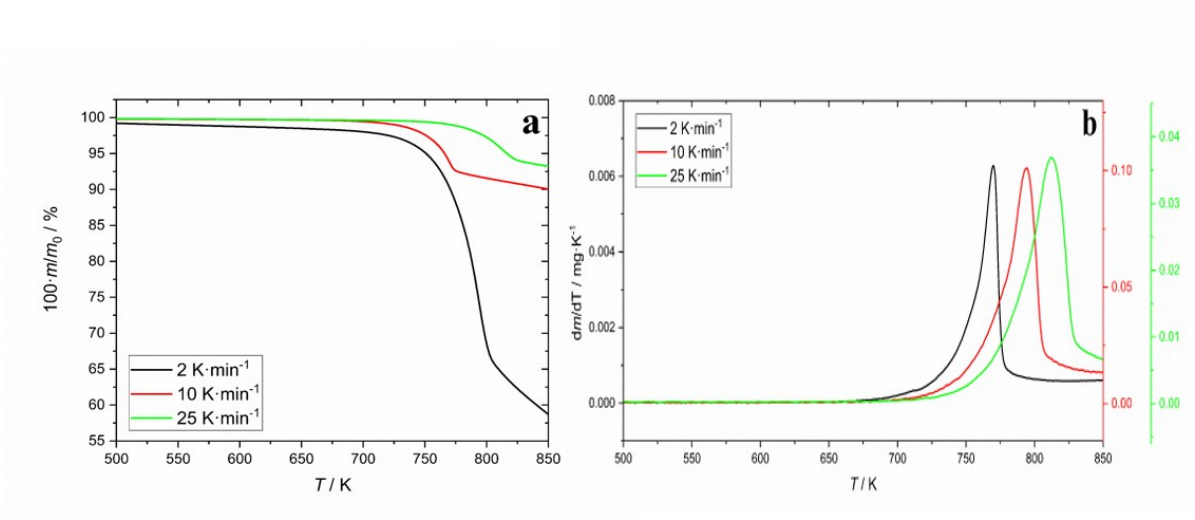

Fig. S7 TGA and corresponding DTG curves for the thermal decomposition of guanine under linear non-isothermal conditions and under N_2 flow (200 ml·min^{-1}).

We can observe from **Fig. S3** – **Fig. S7** that the total mass loss of each nucleobase is increasing with decreasing heating rate. This behavior can be explained by the fact that not only thermal decomposition is measured during the non-isothermal scan of nucleobases in TGA. In fact, thermal decomposition of nucleobases is also superposed with the sublimation of the still non decomposed material, therefore, if we use low heating rate we increase the sublimation time and we will have more mass loss and if we use higher heating rate we will decrease the sublimation time and we will have lower mass loss.

Due to the comparatively slow heating rates (2, 10 and 25 K·min^{-1}), the thermal decomposition of the solid-state nucleobases takes place as a single mass loss step below the fusion temperature (see **Fig. S3** – **Fig. S7**). Thus, we can affirm that we are investigating decomposition without the effect of melting.

TGA data were subjected to isoconversional kinetic analysis. The TGA is the most common thermal analysis technique used to study thermal degradation of polymers and organics, it was demonstrated to be an effective tool for studying complex kinetics.[9] The dependence of the activation energy E_α, the pre-exponential factor A_α and the integral form of the reaction model $g(\alpha)$ with the conversion α were determined through this study. The conversion α is readily determined as a fractional change of any physical property associated with the reaction progress. When the process progress is monitored as a change in the mass by TGA, α is determined as a ratio of the current mass loss Δm to the total mass change Δm_{tot} occurred throughout the process eq. (S1):

$$\alpha = \frac{m_0 - m\,(T)}{m_0 - m_\infty} = \frac{\Delta m}{\Delta m_{tot}} \tag{S1}$$

An advanced isoconversional method developed by Vyazovkin[10,11] was applied to determine the dependence of the activation energy E_α with the extent of conversion α. The method employs a numerical algorithm that was developed under the basic isoconversional assumption that for any given α, $g(\alpha)$ remains unchanged when changing the temperature program. The activation energy E_α is found as the value that minimize the objective function eq. (S2):

$$\Phi(E_\alpha) = \sum_{i-1}^{n}\sum_{j\neq i}^{n}\frac{J[E_\alpha, T_i(t_\alpha)]\beta_j}{J[E_\alpha, T_j(t_\alpha)]\beta_i} \tag{S2}$$

$$J[E_\alpha, T_i(t_\alpha)] = \int_{T_{\alpha-\Delta\alpha}}^{T_\alpha} exp\left[\frac{-E_\alpha}{RT_i(t_\alpha)}\right]dT \tag{S3}$$

To complete the determination of the whole kinetic triplet (E_α, A_α, $g(\alpha)$), the pre-exponential factor A_α and the integral form of the reaction model $g(\alpha)$ were calculated using another isoconvertional method. For non-isothermal conditions, there are several relationships used to compute the pre-exponential factor A_α and $g(\alpha)$, each of them is based on an approximate form of the temperature integral.[12-14] One of such approximations gives rise to the Coats Redfern equation [15-17] see eq. (S4). This method is reported[18] to be one of the most frequently used to evaluate non-isothermal kinetic data. The results of the kinetic triplet are summarized in **Table S3**.

$$\ln\left[\frac{g(\alpha)}{T_\alpha^{\,2}}\right] = \ln\left(\frac{A_\alpha R}{\beta E_\alpha}\right)\left(1 - \frac{2RT_\alpha}{E_\alpha}\right) - \frac{E_\alpha}{RT_\alpha} \tag{S4}$$

where β is the heating rate and T_α is the temperature that correspond to the conversion α.

Table S3 Kinetic parameters of the thermal decomposition of the studied nucleobases.

Compound	$E_{\alpha,mean}$[a]/ $kJ \cdot mol^{-1}$	$\log_{10}\left(A_\alpha/s^{-1}\right)$ [b]	$g(\alpha)$ [c]
uracil	237 ± 20	17.0	$1-(1-\alpha)^{2/3}$
thymine	186 ± 13	12.7	$1-(1-\alpha)^{2/3}$
cytosine	254 ± 15	19.7	$1-(1-\alpha)^{2/3}$
adenine	188 ± 6	12.6	$1-(1-\alpha)^{2/3}$
guanine	306 ± 4	17.8	$1-(1-\alpha)^{2/3}$

[a] Mean activation energy. [b] Logarithm of the pre-exponential factor. [c] The integral reaction model.

With the help of the evaluated decomposition parameters, we solved the reversed task of the isoconversional kinetics and simulated the decomposition reaction at the heating rates of conventional DSC and FSC. The dependence of the temperature T_α with the conversion α at the required heating rate β was calculated by numerical solution of the following equation:

$$g(\alpha) = \frac{A_\alpha}{\beta}\int_0^{T_\alpha} exp\left[\frac{-E_\alpha}{RT_\alpha}\right]dT \qquad \text{(S4)}$$

The results of the numerical resolution of eq. (S5) are shown for uracil in **Fig. S8**a. The computed $\alpha - T_\alpha$ data were fitted with a sigmoidal curve to extrapolate to lower and higher temperatures and the derivative of the computed data and the fitting sigmoid are shown in **Fig. S8b**.

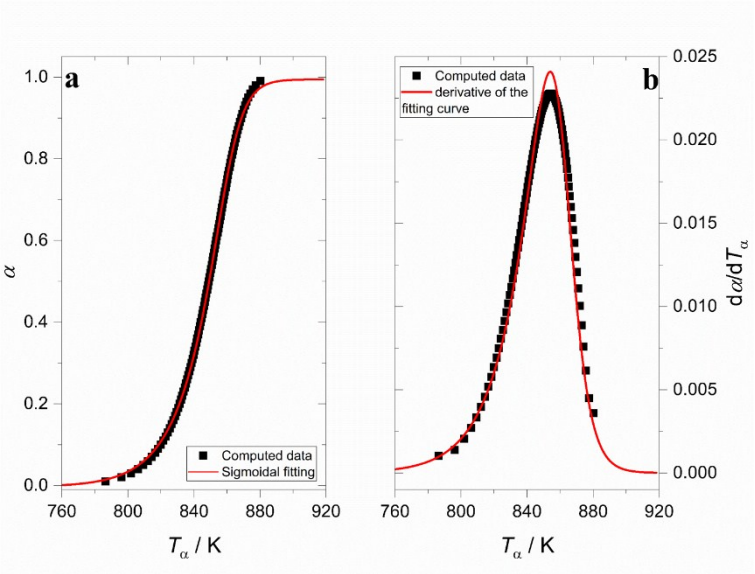

Fig. S8 a) Thermal decomposition of uracil at 8000 $K \cdot s^{-1}$: temperature dependence of conversion is given as black squares and the fitting results are presented by the sigmoidal red line b) First derivative from the conversion temperature dependence is given as black squares and the fitting results of the first derivative are presented as the Gaussian like red line.

The melting peak and the simulated thermal decomposition peak at fast heating rate (8000 $K \cdot s^{-1}$) for uracil, are shown in **Fig. S9**. The two processes take place within different not overlapping temperature ranges, we denote that the thermal decomposition shifts to higher temperatures when using high heating rates and this result proves that high heating rates are needed to get the full melting of thermally instable compounds not superposed by any competitive chemical reaction processes like thermal decomposition. The onset of the melting peak observed in FSC (T_{onset}) and the start temperature of the simulated thermal decomposition peak ($T_{start,dec}$) for all nucleobases are listed in **Table S4**.

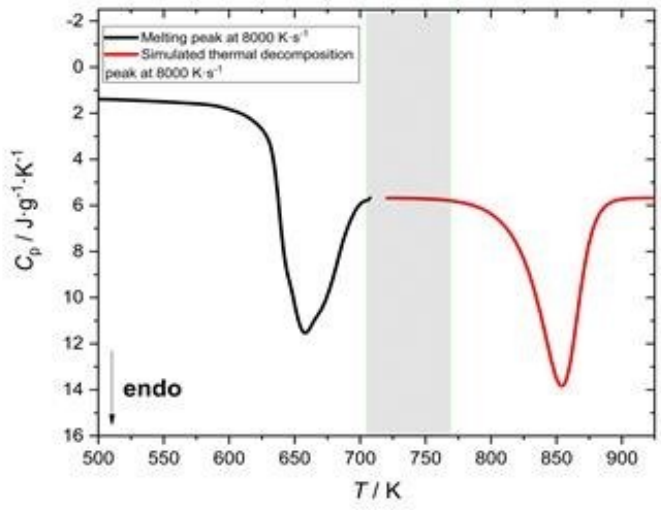

Fig. S9 Superposed melting peak and simulated rescaled thermal decomposition peak for uracil both at heating rate of 8000 $K \cdot s^{-1}$.

Table S4 The onset temperature of the melting peak T_{onset} and the onset of the simulated thermal decomposition peak $T_{start,dec}$ at the corresponding heating rates β used to study melting of nucleobases.

Compound	β/ $K \cdot s^{-1}$	$T_{onset,}$[a]/ K	$T_{start,dec}$[b]/K	T_m [c]/ K
uracil	8000	624	769	610
thymine	8000	599	785	596
cytosine	6000	611	751	606
adenine	8000	652	802	646
guanine	30000	891	948	862

[a] Melting onset for the corresponding fast heating rate. [b] Thermal decomposition onset for the corresponding fast heating rate. [c] Fusion temperatures measured in this work by the FSC and extrapolated to zero heating rate.

The fast heating in FSC shifts the decomposition reaction to higher temperatures providing a close to 100 K temperature gap between melting and decomposition peaks, what assures the determination of the "pure" fusion characteristics not superimposed with decomposition processes.

REFERENCES

1. R. D. Stiehler and H. M. Huffman, *J. Am. Chem. Soc.*, 1935, **57**, 1741-1743.
2. V. N. Emel'yanenko, D. H. Zaitsau, E. Shoifet, F. Meurer, S. P. Verevkin, C. Schick and C. Held, *J. Phys. Chem. A*, 2015, **119**, 9680-9691.
3. X.-Y. ZHANG, B. XUE, Z. CHENG, Z.-C. TAN and Q. SHI, *Acta Phys. Chim. Sin.*, 2015, **31**, 412-418.
4. J. S. Boyer, M. R. Francis and J. Boerio-Goates, *J. Chem. Thermodyn.*, 2003, **35**, 1917-1928.
5. A. Abdelaziz, D. H. Zaitsau, T. Mukhametzyanov, B. Solomonov, P. Cebe, S. P. Verevkin and C. Schick, *Thermochim. Acta*, 2017, **657**, 47-55.
6. P. Cebe, B. P. Partlow, D. L. Kaplan, A. Wurm, E. Zhuravlev and C. Schick, *Thermochim. Acta*, 2015, **615**, 8-14.
7. G. W. H. Hohne, W. Hemminger and H. J. Flammersheim, *Differential Scanning Calorimetry - An Introduction for Practitioners*, Springer, Berlin, 1996.
8. Y. Corvis, A. Wurm, C. Schick and P. Espeau, *J. Phys. Chem. B*, 2015, **119**, 6848-6851.
9. S. Vyazovkin, *Isoconversional Kinetics of Thermally Stimulated Processes*, Springer Switzerland, 2015.
10. S. Vyazovkin, *J. Comput. Chem.*, 1997, **18**, 393-402.
11. S. Vyazovkin, *J. Comput. Chem.*, 2001, **22**, 178-183.
12. T. Ozawa, *Bull. Chem. Soc. Jpn.*, 1965, **38**, 1881-1886.
13. H. E. Kissinger, *Anal Chem*, 1957, **29**, 1702-1706.
14. J. H. Flynn, *Thermochim. Acta*, 1997, **300**, 83-92.
15. A. W. Coats and J. P. Redfern, *Nature*, 1964, **201**, 68-&.
16. E. Urbanovici, C. Popescu and E. Segal, *J. Therm. Anal. Calorim.*, 1999, **58**, 683-700.
17. D. Trache, A. Abdelaziz and B. Siouani, *J. Therm. Anal. Calorim.*, 2017, **128**, 335-348.
18. N. J. Carr and A. K. Galwey, *Thermochim. Acta*, 1984, **79**, 323-370.